

# 3D Face Morphing Attacks: Generation, Vulnerability and Detection

Jag Mohan Singh, *Member, IEEE* Raghavendra Ramachandra, *Senior Member*

**Abstract**—Face Recognition systems (FRS) have been found vulnerable to morphing attacks, where the morphed face image is generated by blending the face images from contributory data subjects. This work presents a novel direction towards generating face morphing attacks in 3D. To this extent, we have introduced a novel framework based on blending the 3D face point clouds corresponding to the contributory data subjects. The proposed method will generate the 3D face morphing by projecting the input 3D face point clouds to depth-maps and 2D color images followed by the image blending and wrapping operations performed independently on the color images and depth maps. We then back-project the 2D morphing color-map and the depth-map to the point cloud using the canonical (fixed) view. Given that the generated 3D face morphing models will result in the holes due to a single canonical view, we have proposed a new algorithm for hole filling that will result in a high-quality 3D face morphing model. Extensive experiments are carried out on the newly generated 3D face dataset comprised of 675 3D scans corresponding to 41 unique data subjects. Experiments are performed to benchmark the vulnerability of the proposed 3D morph generation scheme against automatic 2D and 3D FRS and human observer analysis. We also present the quantitative assessment of the quality of the generated 3D face morphing models using eight different quality metrics. Finally, we have proposed three different 3D face Morphing Attack Detection (3D-MAD) algorithms to benchmark the performance of the 3D face morphing scans generated using the proposed method.

**Index Terms**—Biometrics, Face Recognition, Vulnerability, 3D Morphing, Point Clouds, Image Morphing, Morphing Attack Detection

## 1 INTRODUCTION

Face Recognition Systems (FRS) are being widely deployed in numerous applications related to security settings such as automated border control (ABC) gates and commercial settings like eCommerce and e-banking scenarios. The rapid evolution of the FRS can be attributed to the advances in deep learning FRS [1], [2] which provided improved accuracy in real-world and uncontrolled scenarios. These factors accelerated the use of 2D face images in the electronic Machine Readable Document (eMRTD), which is exclusively used to verify the passport's owner at the various ID services, including border control (both automatic and human). Since most of the countries still use the printed passport images for the passport application process, the face morphing attack has indicated the vulnerability on both human and automatic FRS [3], [4]. Face morphing is the process of blending the multiple face images either based on the facial landmarks [5] or based on the Generative Adversarial Networks [6] to generate the morphing face image. The extensive analysis reported in literature [7], [8], [9], [10] has demonstrated the vulnerability of the 2D face morphing images to both deep learning and commercial-off-the-shelf FRS.

There exist several techniques to detect the 2D face morphing attacks that can be classified as [11] (a) Single image-based Morph Attack Detection (S-MAD): where the face Morphing Attack Detection (MAD) techniques will use the single face image to arrive at the final decision (b) Differential Morphing Attack Detection (D-MAD): where a pair of

2D face images are used to arrive at the final decision. Both S-MAD and D-MAD techniques are extensively studied in the literature that has resulted in several MAD techniques. The reader is advised to refer to the recent survey by Venkatesh et al. [11] to get a comprehensive overview of the existing 2D MAD techniques. Despite the rapid progress in 2D MAD techniques, the recent evaluation report from NIST FRVT MORPH [12] indicates the degraded detection of 2D face morphing attacks. Thus, the 2D MAD attacks, especially in the S-MAD scenario, show significant challenges for reliable detection. These factors motivate us to explore 3D face morphing so that the use of depth information may provide a reliable cue that makes the morphing detection easier.

The 3D face recognition is widely studied from past several decades that has resulted in the several real-life security-based applications with 3D face photo-based national ID cards [13], [14], [15], 3D face photo-based driving license card [15] and 3D face-based automatic border control gates (ABC) [16]. The real case reported in [17] has demonstrated the use of a 2D rendered face image from a 3D face model instead of a real 2D face photo to obtain the ID card bypassing the human observers at the ID card issuing protocol. Although most real-life 3D face applications are based on comparing the 3D face models against 2D face images for verification, this is mainly because epassport uses a 2D face image.

However, the use of 3D to 3D comparison will be realistic, especially in the border control scenario as both ICAO 9303 [18], and ISO/IEC 19794-5 [19] standards are well defined to accommodate the 3D face model in the 3rd generation epassport. The 3D face ID cards are a reality as they are being deployed in the countries like UAE [13]

that can facilitate both human observers and automatic FRS to achieve accurate, secure, and reliable ID verification. Further, the evolving technology has made it possible for 3D face imaging on handheld and smartphones (e.g., Apple Face ID [20] uses 3D face recognition) that can further enable remote ID verification based on the 3D face verification. These factors have further motivated us to investigate the feasibility of generating the 3D face morphing and study their vulnerability and detection.

In this work, we present a novel method for generating 3D face morphing using 3D point clouds. Given the 3D scans from the accomplished and the malicious actors, the proposed method will project the 3D point clouds to the depth-maps & the 2D color images, which are independently blended, warped and back-projected to the 3D to obtain the 3D face morphing. The motivation of projecting to the 2D for morphing is to effectively address the non-rigid registration especially with the high volume of point clouds ( 85K) needs to be registered between two unique data subjects. Further, the use of canonical view generation to project from 3D to 2D and also back project to 3D will assure the high quality depth even for the morphed face images thus it can indicate the high vulnerability on the FRS. Thus, this is the first framework addressing the generation of the 3D face morphing of two unique face 3D scans that can result in the vulnerability with FRS. More particularly, we aim to seek answers to the following research questions, which will be answered systematically in this paper:

- **RQ#1:** Does the proposed 3D face morphing generation technique yield a high-quality 3D morphed model?
- **RQ#2:** Does the generated 3D face morphing model indicate the vulnerability for both automatic 3D FRS and human observers?
- **RQ#3:** Are the generated 3D face morphing models more vulnerable when compared to 2D face morphing images for both automatic 3D FRS and human observers?
- **RQ#4:** Does the 3D point cloud information be used to detect the 3D face morphing attacks reliably?

We systematically address these research questions through our contributions listed as follows:

- We present a novel 3D face morphing generation method based on the point clouds obtained by fusion of depth maps and 2D color images to generate the 3D face morphing model.
- Extensive analysis of the vulnerability of the generated 3D face morphing is studied by quantifying the attack success rate to 3D FRS. The vulnerability analysis is also performed using 2D FRS (both deep learning and COTS).
- Human observer analysis for detecting the 3D face morphing and 2D face morphing is presented to study the significance of depth information in detecting the morphing attack.
- The quantitative analysis of the generated 3D morphed face models is presented using eight different quality features representing both color and geometry.
- We present three different 3D MAD techniques based on the deep features from point clouds to benchmark the 3D face MAD.
- A new 3D face dataset with bona fide and morphed models are developed corresponding to 41 unique data

subjects. The whole dataset had 675 3D scans. We collected a new 3D face dataset as we were interested in capturing high-resolution (suitable for ID enrolment) inner face data [21] Our 3D face dataset consists of raw 3D scans (number of 3D vertices between 31289 & 201065) and processed 3D scans (number of 3D vertices between 35950 & 121088), which is much higher than existing 3D face datasets<sup>1</sup>.

In the rest of the paper we introduce the proposed method in Section 2 and experiments & results in Section 3. This is followed by discussion about the different aspects of the proposed method in Section 4, followed by limitations & potential future-works in Section 5 and finally conclusions in Section 6.

## 2 PROPOSED METHOD

Figure 1 shows the block diagram of the proposed 3D face morphing generation framework based on the 3D point clouds. We are motivated to employ the 3D point clouds over traditional 3D triangle mesh for two main reasons. The first is that connectivity information in a 3D triangle mesh leads to storage overhead, processing, managing, and manipulating the triangular meshes. Thus, the use of 3D triangle meshes will significantly increase both compute and memory, making it less suitable for low-compute devices. The second reason is that the commodity scanning devices (for example, the Artec Sensor) can reproduce detailed colored point clouds that capture both appearance and geometry. Thus, allowing us to generate high-quality 3D face morphing attacks.

3D face morphing generation is challenging in general as it requires a) establishing a dense 3D correspondence between the two contributing data subjects, which is challenging due to less-robust 3D facial key-point detection compared with 2D facial key-point detection, b) estimation of locally affine deformation which is required for non-rigid registration and c) pose misalignment and presence of non-rigid deformation between the two contributing data subjects would reduce the chances of convergence of the global optimization [22], [23], [24]. Further, 3D point clouds have particular challenges as follows a) Robust Detection of 3D facial key-points using point clouds of faces compared to triangle meshes and b) Presence of a higher amount of noise compared to triangle meshes as point cloud data could be output from the 3D scanner directly without cleanup.

The crucial part of the 3D morphing using point clouds is reliable alignment before performing the morphing operation. Given the 3D face point clouds on source and the target face, the point cloud registration can be defined as aligning a source point cloud to a target point cloud. The point cloud registration can be grouped into three broad categories [25] namely 1) Deformation Field, 2) Extrinsic Methods and 3) Learning-based methods. Deformation Field-based techniques could be defined as the computation of deformation between the two-point clouds, which can be achieved either by assuming pointwise position [26] variables or by pointwise affine transformations [27]. Pointwise position

1. The reader is referred to Table 1 of 3D face datasets (inner face data only) from the survey by Egger et al. [21]

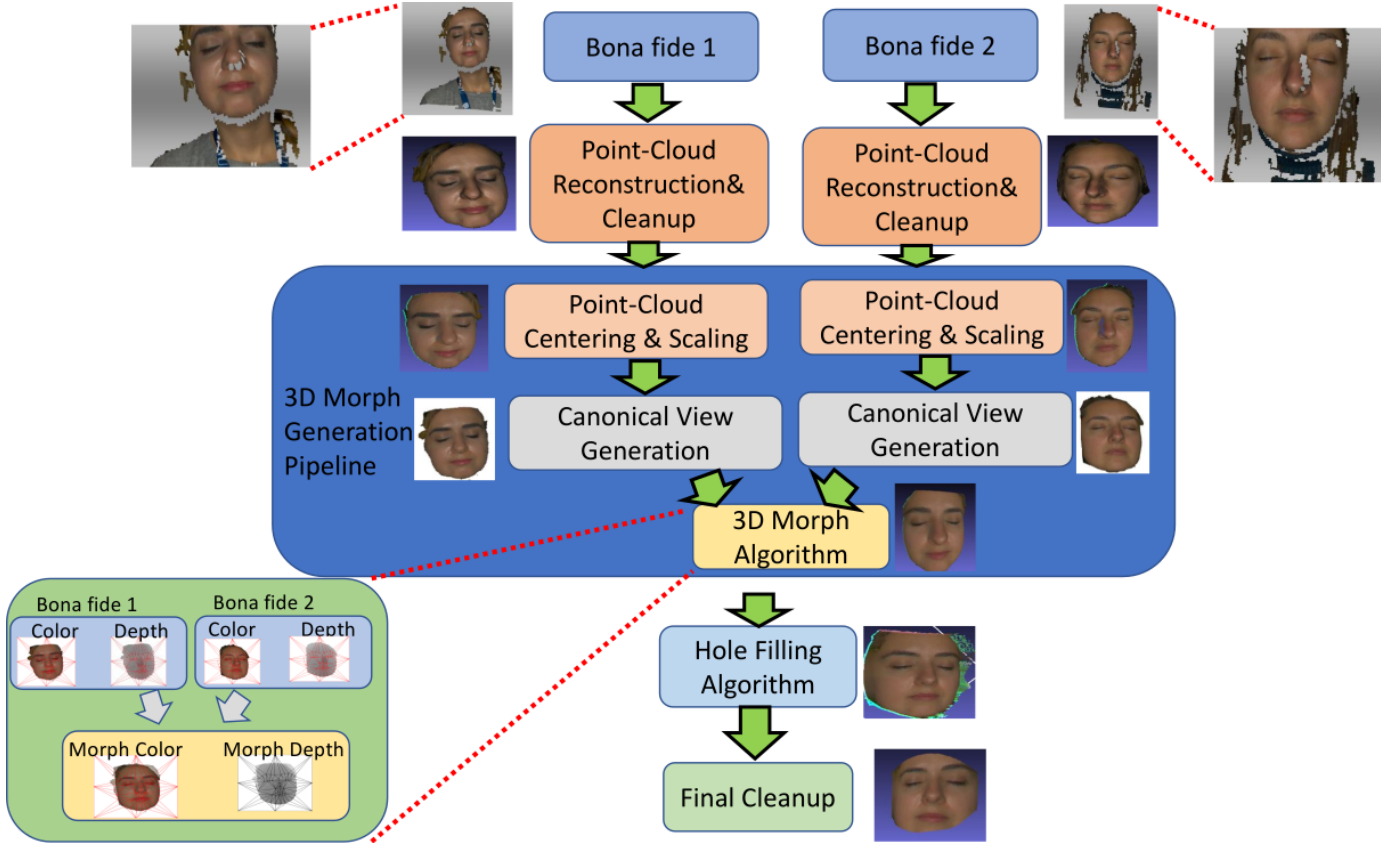


Fig. 1. Block diagram of the proposed 3D face morphing generation technique

variables methods are simplistic as they don't model deformations compared with pointwise affine transformations, which model local rotations. However, since the local transformations need to be stored and computed at a per-point level, this results in high computational and memory costs. This limitation was overcome by deformation field-based methods by use of deformation graph embedding over the initial point set, which consists of fewer nodes than the underlying point set [28], [29].

Extrinsic methods are based on the optimization of an energy function to compute the point set correspondence which usually includes an alignment term and a regularization term [28]. However, the optimization-based methods compute deterministic modeling of the transformation. Probabilistic modeling of transformation was done by Myronenko et al. [30] in their algorithm Coherent Point Drift (CPD) which assumes the source points to be centroids of equally-weighted Gaussian with isotropic covariance matrix in Gaussian Mixture Model (GMM). CPD consists of both alignment and regularization terms for the computation of transformation and performs non-rigid registration but has memory and compute cost. However, the main limitation of optimization-based methods is that they produce good results when the input surfaces are close. Further, they require good initialization of the correspondences otherwise, they can converge to local minima. This was overcome by Learning-based methods, which are data-driven and are of two types (1) Supervised methods and (2) Unsupervised methods. Supervised methods require ground-truth data

for training [31] but can work with varying point cloud density and underlying geometry. Unsupervised methods don't require ground-truth data and can be trained by use of a deformation module based on CNN, followed by an alignment module to compute the deformation [32].

However, the use of existing point cloud registration for this precise application of 3D face morphing point cloud generation will pose challenges such as: **registration using the same individual**: Point cloud registration has mainly focused on the non-rigid registration of two-point clouds from the same individual [25]. This is primarily because high-quality registration aims to produce a globally consistent 3D mesh. Thus, the registration methods have not been tested in the scenario where two different point clouds are registered compared to those from the same individual. **Vertex accurate correspondence**: 3D Face Morphing requires perfect vertex correspondence between the source and target point clouds, which is challenging and has not been evaluated extensively. **Low vertex count point clouds**: Point cloud registration, especially using learning-based methods, has network architectures based on point clouds with a low number of vertices ( 1024). Thus, registering point clouds with many vertices ( 75K) has not been evaluated extensively and thus suitable for low resolution face images. To effectively address these challenges, the proposed method consists of four stages, including (1) point cloud reconstruction and cleanup, (2) 3D morph generation, (3) hole-filling algorithm, and (4) final cleanup. In the following subsections, these steps are discussed in detail.

## 2.1 Point Cloud Reconstruction & Cleanup

We capture a sequence of raw 3D scans using Artec Eva sensor [33] from two different data subjects that are to be morphed ( $S_1$  and  $S_2$ ). In this work, we consider the case of morphing two data subjects at a time because of its real-life applications, as demonstrated in several 2D face morphing works [3], [11]. We process both  $S_1$  and  $S_2$  by performing a series of pre-processing operations such as noise filtering, texturing, and fusion of input depth maps to generate the corresponding point clouds  $P_1$ , and  $P_2$ . These operations are carried out using Artec Eva Studio SDK filters together with the Meshlab filter [34]. The cleaned and process point clouds are qualitatively shown in Figure 1.

## 2.2 3D Morph Generation Pipeline

In the next step, we process the point clouds  $P_1$ , and  $P_2$  to generate a 3D face morphing point cloud by following series of operations which are discussed below:

### 2.2.1 Point-Cloud Centering & Scaling

We first compute the minimum enclosing spheres using the algorithm from Gärtner et al. [35] to get the two bounding spheres with centres and radii ( $C_1, r_1$ ), & ( $C_2, r_2$ ) corresponding to the point cloud  $P_1$ , and  $P_2$  respectively. Note  $P_1 = (v_1^1, \dots, v_1^{n1})$  where  $v_1^i$  is the  $i^{\text{th}}$  3D vertex, and  $n1$  is the number of points in the point cloud  $P_1$ , and  $P_2 = (v_2^1, \dots, v_2^{n2})$  where  $v_2^i$  is the  $i^{\text{th}}$  3D vertex, and  $n2$  is the number of points in the point cloud  $P_2$ . We then subtract the sphere center  $C_1$  from each 3D vertex of  $P_1$  and we repeat the same operation on  $P_2$  with  $C_2$ . Finally, the centered point clouds are further scaled to the common radius which normalizes the 3D point clouds to the common scale. The resulting centered and scaled point clouds corresponding to  $P_1$  and  $P_2$  are denoted as  $PC_1$ , and  $PC_2$ , respectively. The qualitative result of this operation is as shown in the Figure 1 that shows centered and scaled 3D point clouds.

### 2.2.2 Canonical View Generation

This step performs the fine alignment by projecting the 3D face point clouds  $PC_1$  and  $PC_2$  to the canonical view (or the fixed virtual view). The canonical view (or the fixed virtual view) is defined so that the virtual camera parameters used for projecting 3D Point Cloud to 2D Color Image and Depth Map projection are identical for the entire dataset. The canonical view is chosen, so that majority of faces have a frontal view. This step aims to keep the view and projection matrix identical to the 3D face point clouds  $PC_1$  and  $PC_2$ . We then project  $PC_1$  and  $PC_2$  to generate 2D color images and depth maps using the canonical view parameters. The generated 2D color images and depth maps are denoted as  $(I_1, D_1)$  and  $(I_2, D_2)$  that corresponds to the point clouds  $PC_1$ , and  $PC_2$  respectively. We mainly chose the canonical view for projecting 3D point clouds to 2D color images and depth maps due to lack of initial alignment estimation required for non-rigid global registration methods such as by Li et al. [23]. Further, as the human face's frontal profile can be considered a 2D height-map thus, a single 2D color image and depth map represent it without losing any information.

The qualitative results of the canonical view transformation are shown in Figure 1 which demonstrates the aligned

2D color images, and depth maps zoomed in the inset image.

---

### Algorithm 1 3D Face Morphing Algorithm

---

**Input** ( $I_1, I_2, D_1, D_2, CV$ )

**Output** ( $P_M$ )

- 1: Detect Facial Keypoints on  $K_1$  on  $I_1$ , and  $K_2$  on  $I_2$  using Dlib [39], and generate key-points of the morph using Equation 1.
- 2: Perform Delaunay Triangulation on  $K_M$  which is obtained by blending  $K_1$  and  $K_2$  using Equation 1.
- 3: Estimate Affine Warping between corresponding triangles of  $K_1$  &  $K_M$  denoted as  $w_1^M$ , and for  $K_2$  &  $K_M$  denoted as  $w_2^M$ .
- 4: Apply affine warping  $w_1^M$  on  $I_1$  to obtain  $I_{1M}$ , and on  $D_1$  to obtain  $D_{1M}$ .
- 5: Apply affine warping  $w_2^M$  on  $I_2$  to obtain  $I_{2M}$ , and on  $D_2$  to obtain  $D_{2M}$ .
- 6: Obtain morphed color image  $I_M$  using the warped key-points from the color images  $I_1$ , and  $I_2$  using Equation 1, and morphed depth map  $D_M$  using Equation 2.
- 7: Obtain the morphed point cloud by back-projecting  $I_M$ , and  $D_M$  to obtain the colored 3D point cloud  $P_M$  with 3D coordinates  $\forall i \in \{1, \dots, n3\} (x_i, y_i, z_i) = (x_i, y_i, D_M(x_i, y_i))$  and color  $\forall i \in \{1, \dots, n3\} \text{Color}(x_i, y_i, z_i) = C_M(x_i, y_i)$  where  $n3 = \min(n1, n2)$ .

---

### 2.2.3 3D Morph Generation

Given the 2D face color images  $(I_1, I_2)$  and depth-maps  $(D_1, D_2)$  corresponding to  $PC_1$ ,  $PC_2$ . We perform the morphing operation as explained in the Algorithm 1. The primary idea is to perform the morphing in 2D and back-project to 3D. The primary motivation of using a 2D morph generation method is to address the challenge of finding correspondence between  $PC_1$  and  $PC_2$ . The underlining idea is to perform the steps of morphing (facial landmark detection, Delaunay triangulation, & warping) on 2D color images and re-use the same (facial landmark locations, triangulation, and warping) on the depth maps. In this work, we have used the blending (morphing) factor ( $\alpha$ ) as 0.5 as it is well demonstrated to be highly vulnerable in the earlier works on 2D face morphing [6]. The morphing is carried out as mentioned in the equation below:

$$\begin{aligned} I_M &= \alpha \times I_1(K'_1) + (1 - \alpha) \times I_2(K'_2) \\ K'_1 &= w_1^M(K_1) \\ K'_2 &= w_2^M(K_2) \end{aligned} \quad (1)$$

$$K_M = \alpha \times K_1 + (1 - \alpha) \times K_2$$

where  $\alpha$  is the blending factor,  $K_1$  denotes 2D facial landmark locations corresponding to  $I_1$ ,  $K_2$  denotes 2D facial landmark locations corresponding to  $I_2$ ,  $K_M$  is generated by blending  $K_1$ , &  $K_2$ ,  $w_1^M$  denotes the warping function from  $K_1$  to  $K_M$ ,  $w_2^M$  denotes the warping function from  $K_2$  to  $K_M$ , and  $I_M$  is the morphed 2D color image. Similarly, the same operations are carried out on the depth maps as shown in the equation below:

$$D_M = \alpha \times D_1(K'_1) + (1 - \alpha) \times D_2(K'_2) \quad (2)$$

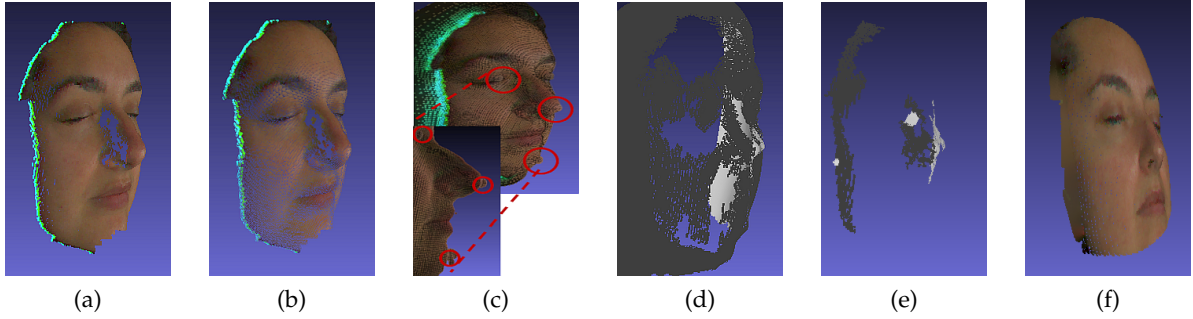


Fig. 2. Qualitative results of the hole filling algorithms (a) Input Point Cloud with holes, (b) Point Cloud with Normals which has noise, (c) Point Cloud with Screened Poisson Reconstruction [36] where artifacts are shown in the inset, (d) Point Cloud Reconstructed with APSS [37], (e) Point Cloud Reconstructed with RIMLS [38], (f) Point Cloud Hole Filled using Proposed Method

where  $D_M$  is the morphed depth-map.

In the next step, we back-project  $I_M$ , and  $D_M$  to get the 3D face morphing point cloud  $P_M = (v_M^1, \dots, v_M^{n3})$  where  $n3 = \min(n1, n2)$  is the number of vertices. Note each 3D vertex is obtained using  $i = 1^{n3}(x_i, y_i, z_i) = (x, y, D_M(x, y))$  and the qualitative results is shown in Figure 1. However, generating the 3D face morphing will result in multiple holes due to a single canonical view. These holes are visible from the other views. Therefore, we present a novel hole-filling algorithm further to improve the perceptual visual quality of the 3D face morphing.

#### Algorithm 2 Hole Filling Point Cloud

---

**Input (n4-views)**  
**Output ( $C_{hf}, D_{hf}, P_{hf}$ )**

- 1: Generate  $n$  pairs of color-maps, and depth-maps  $\{(C_1, D_1), (C_2, D_2), \dots, (C_j, D_j), \dots, (C_{n4}, D_{n4})\}$ , translated from the canonical view.
- 2: **for**  $j \leftarrow 1$  to  $n4$  **do**
- 3: Perform Image In-painting [40] on  $C_j$ , and  $D_j$ .
- 4: Perform Image Registration of  $C_j$  with the canonical view-point color-map  $C_{CV}$  using the following steps:
- 5: Feature Computation using Oriented FAST and Rotated BRIEF (ORB) Descriptor [41].
- 6: Brute-Force Matching of features using Hamming Distance.
- 7: Homography computation using inlier features.
- 8: Perspectively warp the color-map, and the depth-map using computed homography.
- 9: **end for**
- 10: Average all the registered color-maps ( $C_{hf}$ ) and the depth-maps ( $D_{hf}$ ).
- 11: Back-Project the averaged color-map and depth-map from 2D to 3D to generate hole-filled point cloud ( $P_{hf}$ ) using the canonical view parameters.

---

### 2.3 Hole Filling Algorithm

Since the proposed method for 3D face morphing currently uses a single canonical view for projecting input 3D point cloud to 2D color image and depth map. Thus, during back-projection, i.e., generation of the 3D point cloud using a 2D

color image and depth map based on a single canonical view, would result in holes from camera views different from this one. Thus, we need a hole-filling method to generate a point cloud without holes in multiple views. In this step, we propose a new hole-filling algorithm tailored to this specific 3D face morphing generation problem. Since the holes are visible from different views, filling the holes in these views is necessary to improve the perceptual visual quality. Therefore, we transform the 3D face morphing point cloud  $P_M$  multiple times independently to generate  $P_M^j$  where  $j = 1 \dots n4$  and  $n4$  is the number of transformations and each transformation is a 3D translation [42]. In this work, we empirically choose the number of 3D translations to 7 to balance computational cost and the visual quality achieved after the hole filling. Using more 3D translations will significantly increase the computational cost and fail to improve the visual quality. In fact, we attempted the conventional approach of hole filling using 3D triangulation of 3D point cloud proposed in [36], [37], [38].

Figure 2 shows the qualitative results of three different SOTA triangulation algorithms that indicate the non-satisfactory results. This is because 3D orientation (3D normal) estimation indicates artifacts in the 3D triangulated mesh. Therefore, filling holes directly in the 3D point cloud is challenging, as the underlying surface (manifold) is not known in advance. The errors in 3D orientation estimation make it difficult to employ the conventional 3D hole filling approaches. This has motivated us to devise a new approach to achieve effective hole filling. To this extent, we project each point cloud  $P_M^j$  to the 2D face morphing color image ( $C_j$ ) and its corresponding depth-map ( $D_j$ ). We fill the holes in  $C_j$  &  $D_j$  using steps 2 to 9 described in Algorithm 2. Finally, we obtain the hole-filled 3D face morphing point cloud ( $P_{hf}$ ) as indicated in steps 10 and 11 in Algorithm 2. Figure 2 (e) shows the qualitative results of the proposed hole filling that indicated the superior visual quality compared to the existing methods.

### 2.4 Final Cleanup Algorithm

The final cleanup is performed using a clipping region outside a portion of the bounding sphere. The final result from our proposed 3D face morphing, a point cloud, is shown in Figure 3 for a few data subjects<sup>2</sup>.

2. Supporting Video is available at <https://folk.ntnu.no/jagms/SupportingVideo.mp4>

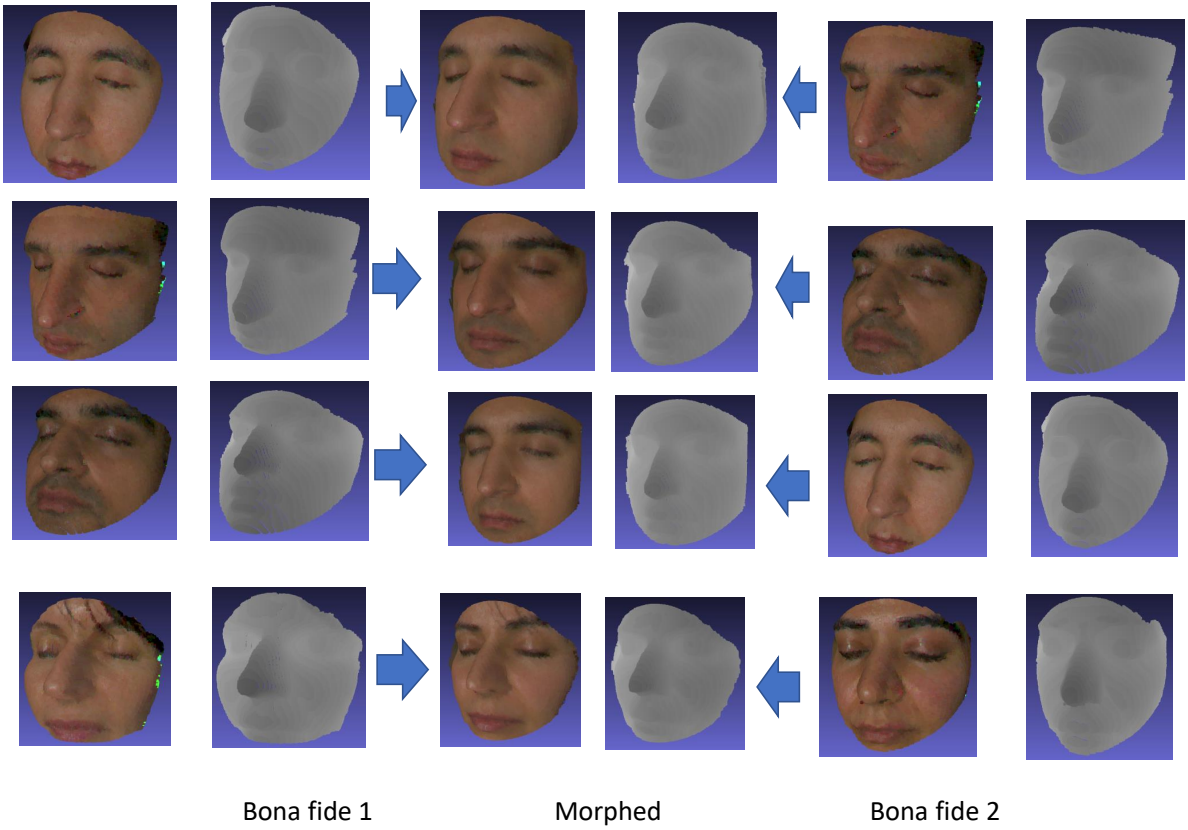


Fig. 3. Illustration of 2D color image and depth maps for bona fide and morphs generated using the proposed method

## 2.5 Qualitative and Quantitative Comparison of Proposed Method with SOTA

To illustrate the effectiveness of the proposed method, we selected few SOTA methods based on non-rigid point cloud registration and methods generating 3D face model from a 2D face image. Our current evaluation of SOTA for Non-Rigid Point Cloud Registration (NRPCR) methods includes CPD by Myronenko et al. [30] and Cornet3D by Zeng et al. [43]. CPD is based on optimization and Cornet3D is a most recent unsupervised deep learning-based method for NRPCR. We also selected two other methods that includes 3DMM [44] and FLAME [45]. These methods are based on converting the 2D face to 2D face models. The 3DMM introduced the concept of morphable model where the parameters such as shape and texture can be controlled during 3D face synthesis. The FLAME technique enhanced the quality of the generated 3D face model from a 2D face image by using more controllable parameters such as pose, expression, shape and texture during 3D face synthesis process.

Figure 4 shows the qualitative results of the proposed method together with four different non-rigid point cloud. The results of qualitative comparison with SOTA are shown in Figure 4. It can be noticed from Figure 4 that all four existing methods fails to indicate the identity features with the generated 3D face morphing model. However, CPD method fails with the alignment of the two input point clouds which results in double features such as eyebrows.

Cornet3D produces lower quality results which can be attributed to the fact that the technique is not focused on face registration exclusively. Similar qualitative results can also be noted with the 3DMM and FLAME where the generated 3D face morphing fails to preserve the identity features that are essential to the improve the attack potential of the 3D face morphing.

To effectively analyse the attack potential of the generated 3D face morphing face, we present the vulnerability analysis with two different 3D face recognition systems namely LED3D [46] and Pointnet++ [47]. Figure 5 shows the scatter plot of the comparison score corresponding to the generated 3D face morphing. The red line in the Figure 5 indicates the threshold of the 3D FRS set at FAR = 0.1%. The given 3D face morphing is said to be vulnerable iff. the comparison scores from corresponding 3D face from both the contributory data subjects exceed the threshold. Thus, the more comparison scores in top right coordinate higher is the vulnerability. As noticed in the Figure 5, the existing methods fails contribute to the vulnerability when compared to the proposed method. Hence, the proposed method is justified to generate the 3D face morphing samples with high attack potential. The low attack potential of the existing methods can be attributed to the low-resolution of the identity specific depth generation by the SOTA as shown in Figure 6

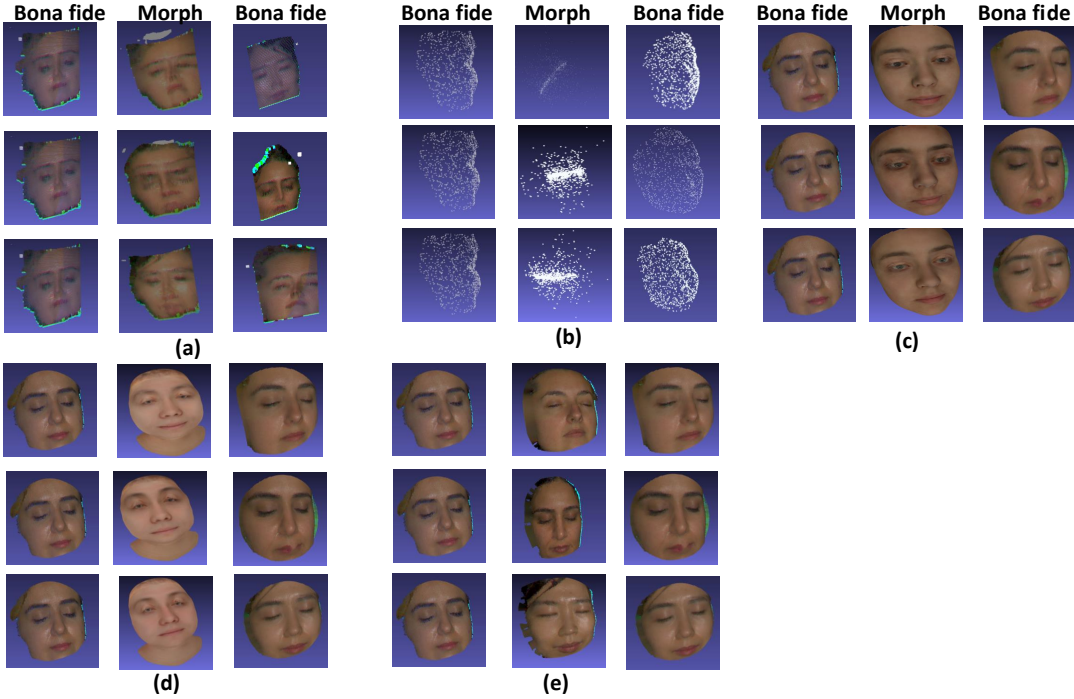


Fig. 4. Illustration of the SOTA Comparison showing Bona fide and Morphs generated using (a) CPD [30], (b) Cornet3D [43], (c) 3DMM [44] (d) FLAME [45] and (e) Proposed Method. Note both 3DMM and FLAME just need a single image as input, and in current evaluation we pass a 2D rendering generated using the proposed method. Note the proposed method shows both high-quality rendering and identity features of the 2D face morphing image. We have evaluated SOTA comparison with three randomly selected samples from our dataset.

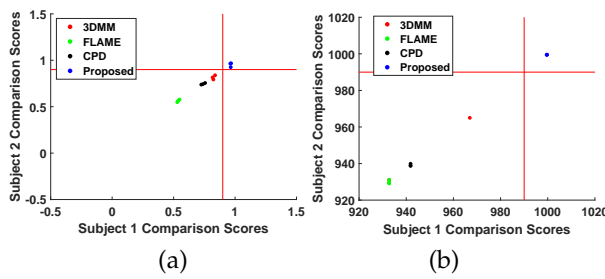


Fig. 5. Illustration showing scatter plot of Comparison scores using Bona fide and Morphs generated using Proposed Method (a) LED3D [46] and (b) Pointnet++ [47] based where SOTA algorithms are 3DMM [44], FLAME [45], CPD [30].

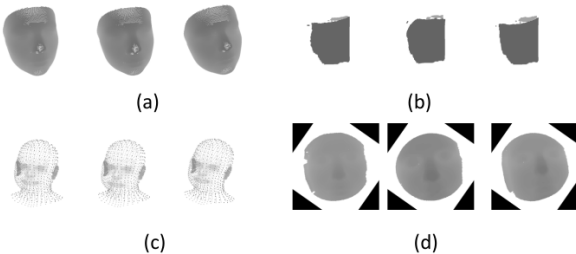


Fig. 6. Illustration showing depth maps using SOTA and proposed method (a) 3DMM [44], (b) CPD [30], (c) FLAME [45] and (d) Proposed Method.

### 3 EXPERIMENTS AND RESULTS

In this section, we present the discussion on extensive experiments carried out on the newly acquired 3D face dataset. We discuss the quantitative results of the various experiments, including vulnerability study on automatic FRS and human observer study, quantitative quality estimation based on color and geometry of the generated 3D face morphing models and automatic detection of 3D MAD attacks.

3D face Bona fide		
Total Data Subjects	Males	Females
41	28	13
Total 3D samples	Males	Females
330	224	106
3D face Morphs		
Total 3D Morphs	Males	Females
345	278	67

TABLE 1  
Statistics of newly collected 3D face dataset

#### 3.1 3D Face Data Collection

In this work, we have constructed a new 3D face dataset using the Artec Eva 3D scanner [33]. The data collection is carried out in an indoor lighting environment. The data subjects are asked to sit on the chair by closing their eyes to avoid the light's strong reflection from the 3D scanner. The 3D scanner is moved in the vertical direction to capture the 3D sequence.

We have used the Artec Studio Professional 14 for the 3D data collection and processing. We have collected the 3D face data from 41 data subjects which include 28 males and 13 females. We have captured nine to ten samples for each data subject in three different sessions in three days. The statistics of the whole 3D face dataset are summarized in Table 1.

One can argue that we might have used the existing 3D face datasets such as FRGC [48] and BU-3DFE [49]. However, the FRGC dataset provides a single depth map and a color image. Thus, a high-quality point cloud cannot be generated. Further, the dataset has a few misaligned color images and depth maps [50] that will result in a low-quality 3D morphing generation. The BU-3DFE [49] dataset does provide 3D models, but these are perfectly registered, and the capture conditions are identical for all the subjects. This does not model the real-world scenario of capturing 3D point clouds with changes in capture conditions that could happen during data collection. The quality of our 3D face dataset has a much higher number of 3D vertices between 35950 & 121088 for the inner face compared to previous methods [21]. These factors motivated us to generate a new 3D face dataset to enable a high-quality 3D face morphing generation suitable for the ID control scenario.

### 3.2 Human Observer Analysis

We perform the human observer analysis to evaluate the human detection performance of the generated 3D morphs. The survey is set up online<sup>3</sup> and is created using PHP, & HTML-CSS tools. GDPR norms are followed during the survey creation, and participants' email (used only for registration to avoid duplication), gender, & experience with the morphing problem are only recorded. All measures are implemented with full considerations of the anonymity of participants. We have designed the GUI for the human observer study to benchmark the single image morphing detection in this work.

Figure 7 shows the screenshot of the web portal used for the human observer's study. The GUI is designed to display two face images at a time such that one corresponds to the 2D face and another corresponds to the 3D face. Then, the human observer is prompted to independently decide these face images as either morph or bona fide. The human observers are provided with an option to rotate the 3D face in different directions to make their decision effectively. Further, the opportunities to zoom in and zoom out the 3D face model are also provided. We have mainly selected to present both 2D/3D face images for human evaluation at the same time to check whether the 3D information might help detect the morphing attacks. Due to the time factor, we have used 19 bona fide and 19 morph samples independently from 2D and 3D for human observer study. Thus, each human observer has spent around 20 minutes on average to complete this study. The detailed step-wise instructions on using the web portal are made available for every participant beforehand.

The human observer study is carried out using 36 different observers with and without face morphing experience. The quantitative results of the human observer study are

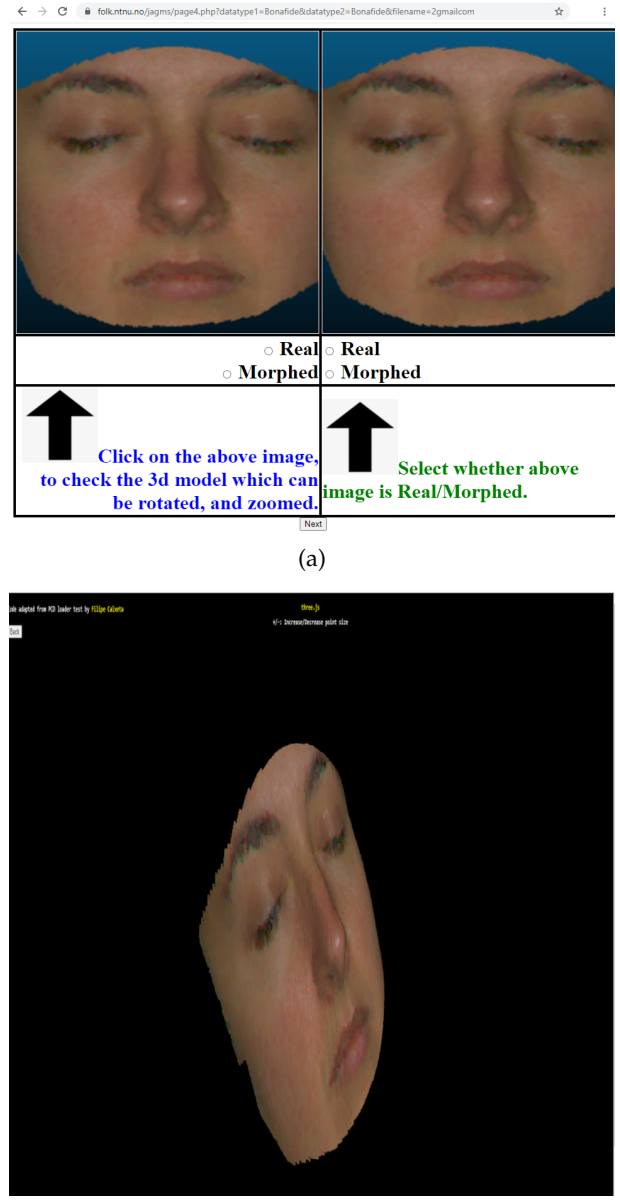


Fig. 7. Screenshots from the GUI of human observer web page (a) Full Page Screenshot, and (b) Screenshot of 3D model page.

shown in Figure 8. We summarize the human observers results from the survey as follows:

- The average detection accuracy of human observers for 2D face bona fide samples is 55.83%, and 42.5% in a 3D face, respectively. The average detection accuracy of human observers for morphs in 2D is 58.33% and 51.85% in a 3D face. Thus, detection accuracy is similar for bona fide and morph in 2D. However, the detection accuracy in 3D is lower for bona fide when compared with morph.
- The average detection accuracy is similar for observers without morphing experience and basic morphing experience. Human observers with advanced morphing experience have the highest average detection accuracy. The observers without morphing experience perform similar to observers with basic morphing experience,

3. <https://folk.ntnu.no/jagms>

Combined			Male		Female	
Algorithm	MMPMR%	FMMPR%	MMPMR%	FMMPR%	MMPMR%	FMMPR%
<b>2D Vulnerability Analysis</b>						
COTS	97.45%	89.78%	97.98%	90.65%	94.03%	86.36%
Arcface	63.81%	28.66%	64.92%	27.13%	59.70%	33.33%
<b>3D Vulnerability Analysis</b>						
LED3D [46]	81.69%	54.00%	82.67%	51.84%	77.61%	63.64%
PointNet++ [47]	95.65%	80.52%	95.32%	79.42%	95.52%	84.85%

TABLE 2

Vulnerability analysis of 2D and 3D FRS, performed on full dataset.

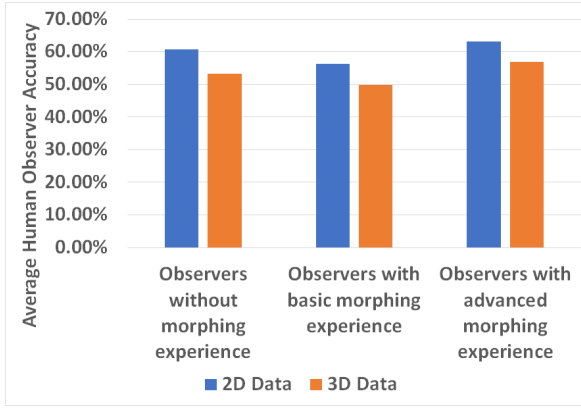


Fig. 8. Illustration of average accuracy of human observer study, note that 2D accuracy is always higher than 3D. It is evaluated using subset of full dataset consisting of 38 bona fide and morph samples.

which can be attributed to the innate human capacity to distinguish between bona fide v/s morphed.

- The survey further validates that generated 3D morphs are challenging to detect from human observations. The average detection accuracy of human observers does not exceed 63.15% which shows that 2D and 3D morphs generated in this work are high quality and difficult to detect.

The average detection accuracy in a 2D face is higher than that in a 3D face, which can be attributed to the following reasons:

- The fact that 2D morph is more prevalent, and thus observers generally look for specific artifacts in different regions of the face makes the task relatively easy with a 2D face.
- The aspect of what artifacts to look at in 3D is unclear to the human observers, as they are not trained for this task.
- The perceptual quality of generated 3D morphs is high, so human observers find it difficult to distinguish the 3D morphs from the 3D bona fide.

### 3.3 Vulnerability Study

In this work, we benchmark the performance of the automatic FRS on both 2D and 3D face models. The 2D face vulnerability is computed using the color image and the 3D face vulnerability is computed based on depth-map/point cloud. We have used two different metrics to benchmark

the vulnerability assessment that includes Mated Morphed Presentation Match Rate (MMPMR) [51] and Fully Mated Morphed Presentation Match Rate (FMMPR) [52]. The vulnerability analysis is performed by enrolling the morphing image (2D/3D) and then obtaining the comparison score by probing both contributory data subjects' face images (2D/3D).

To compute the vulnerability of 2D face morphing images, we have used two different FRS such as Arcface [2] and a Commercial-off-the-Shelf (COTS) FRS <sup>4</sup>. The 3D face vulnerability analysis is performed using Deep Learning-based FRS such as Led3D [46] and PointNet++ [47]. The thresholds for all FRS used in this work is set at FAR=0.1% following the guidelines of Frontex for border control [53]. The results are summarized in Table 2, and the vulnerability plots are shown in Figure 9. Based on the obtained results, it can be noted that (1) Both 2D and 3D FRS are vulnerable to the generated face morphing attacks (2) Among the 2D FRS, the COTS indicates the highest vulnerability compared to the Arcface FRS. (3) Among the 3D FRS the PointNet++ [47] indicates the highest vulnerability. Thus, the quantitative results of the vulnerability analysis indicate the effectiveness of the generated 3D face morphing attacks.

### 3.4 Automatic 3D Face Point Cloud Quality Estimation

In this work, we estimate the visual quality based on the effectiveness of different types of features, including both color and geometry, as proposed in [54]. This study aims to quantitatively estimate the quality of the generated 3D face morphing point clouds and the bona fide 3D face point clouds to quantify the quality of the proposed morphing generation. To this extent, five different point cloud features based on geometry, namely curvature, anisotropy, linearity, planarity, sphericity, and three color information features, namely L color component, A color component, B color component, are computed to benchmark the quality based on the geometry of the generated 3D morphing models.

Figure 10 shows the box plot of the eight different quality metrics for both 3D bona fide and 3D morphing point clouds. The quantitative values (mean and standard deviation) of different quality features are also shown in Table 3. As noted from Figure 9, the quality estimations, mainly based on geometry, indicate the near-complete overlapping for 3D bona fide and 3D morph. Thus, the proposed 3D face morphing generation did not degrade the depth

4. The name of the COTS is not indicated to respect confidentiality

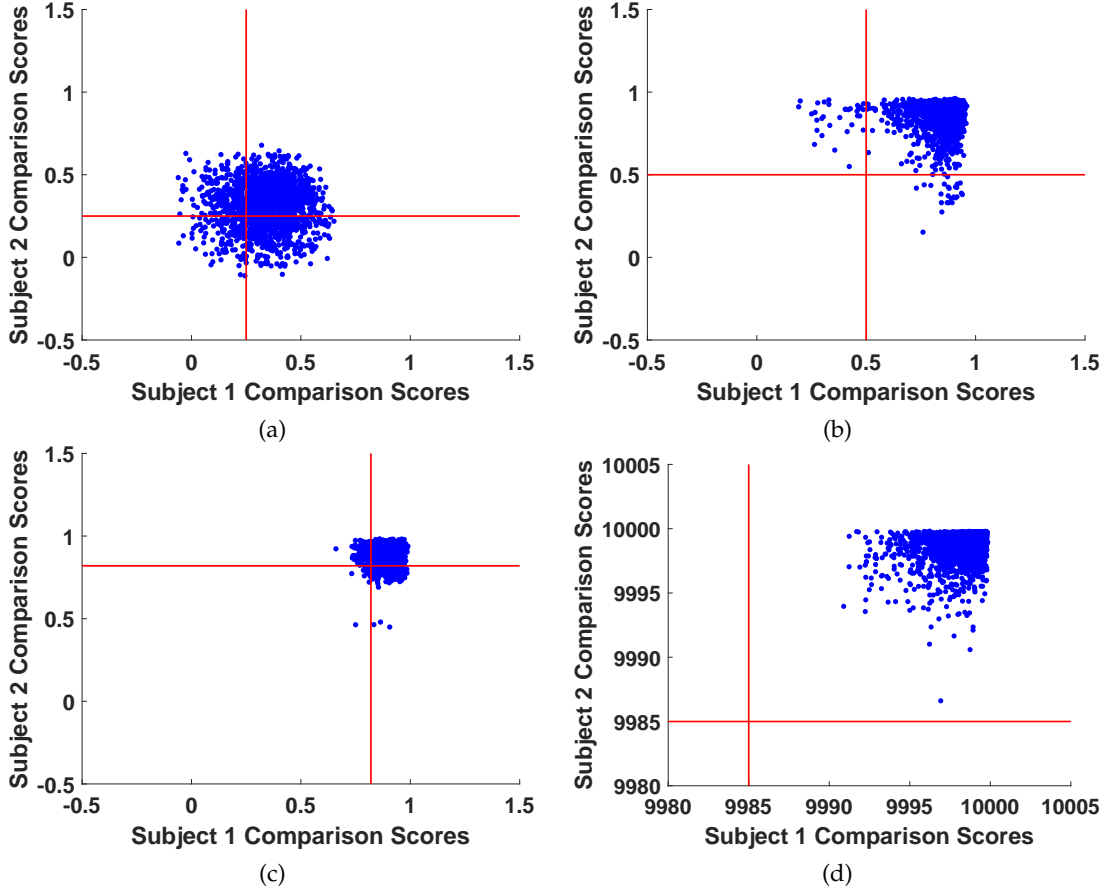


Fig. 9. Vulnerability Plots using 2D & 3D FRS. (a) 2D face FRS using Arcface [2], (b) 2D face FRS using COTS, and (c) 3D face FRS using Led3D [46], and (d) 3D face FRS using Pointnet++ [47]

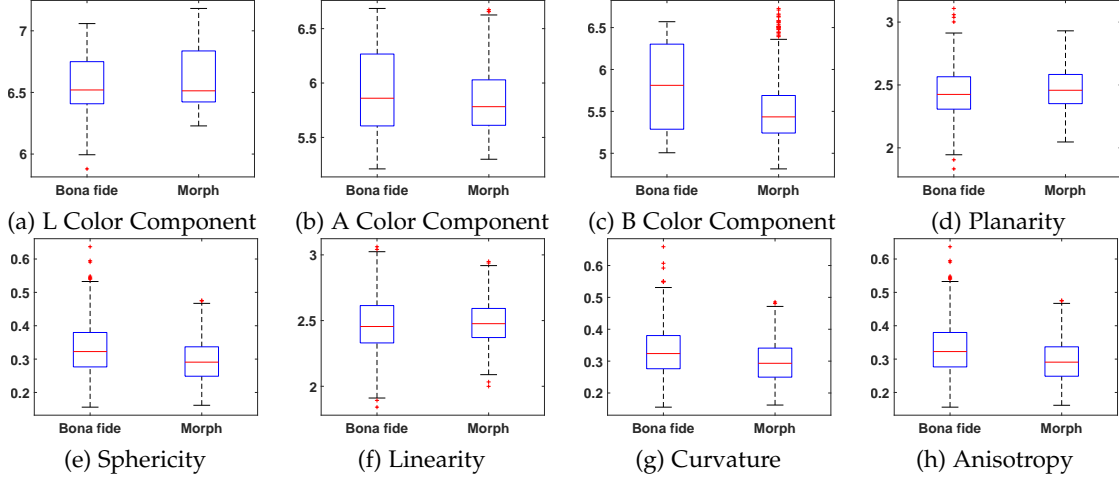


Fig. 10. Box plots showing the eight different 3D model quality estimation from 3D bona fide and 3D morph based on color and geometry, performed on full dataset.

quality. Instead, it has achieved comparable quality based on geometry that of bona fide 3D models used for the morphing operation. Similar observation can also be noted with the color image quality estimation.

### 3.5 3D Face Morphing Attack Detection

In this section, we present our proposed method for a single 3D model-based MAD. Because the 3D face morphing is

extensively presented in this paper for the first time, there exists no state-of-the-art to detect these attacks. Therefore, we are motivated to develop 3D MAD techniques to detect these attacks reliably. The proposed 3D MAD techniques are based on the pre-trained 3D point-based networks that are used to extract the features as shown in Figure 11. Thus, given the 3D face point clouds, we first compute the features from the pre-trained network and in the next step, we feed the same to the linear support vector machine

3D Face Quality Features (mean $\pm$ std. deviation)		Data type	
		Bona fide	Morphed
L Color	6.5614 $\pm$ 0.2191	6.6076 $\pm$ 0.2340	
A Color	5.9368 $\pm$ 0.3547	5.8546 $\pm$ 0.3260	
B Color	5.7998 $\pm$ 0.5074	5.5326 $\pm$ 0.4198	
Linearity	2.4708 $\pm$ 0.2196	2.4911 $\pm$ 0.1776	
Sphericity	0.3318 $\pm$ 0.0807	0.2936 $\pm$ 0.0592	
Anisotropy	0.3318 $\pm$ 0.0807	0.2936 $\pm$ 0.0592	
Curvature	0.3330 $\pm$ 0.0821	0.2965 $\pm$ 0.0606	
Planarity	2.4430 $\pm$ 0.2176	2.4711 $\pm$ 0.1733	

TABLE 3

Quantitative values of quality features for 3D face point clouds corresponding to 3D bona fide and morph based on color and geometry, it evaluated on full dataset, and is evaluated on full dataset.

(Linear SVM) to make the final decision on either bona fide or morph. In this work, we have used three different pre-trained point could networks such as DGCNN [55], Pointnet++ [47], [56] and SimpleView [56] independently to benchmark the 3D MAD performance. All three pre-trained CNNs are trained on ModelNet40 dataset [57]. Pointnet [56], [58] is one of the earliest point-based classifications of deep learning networks invariant to the permutation of 3D vertices. In this work, we use Pointnet++ [47], [56] network and extract Pointnet [56], [58] features from its classification translation layer of 4096 feature-dimensions. DGCNN [55] which introduced edge convolutions for point-cloud segmentation and classification tasks. In the current evaluation, we extract features of 40-dimension from the DGCNN [55] classification task layer. The SimpleView [56] network is based on projecting the point clouds to multiple view depth maps. In this work, given the 3D face point clouds, we extract the features from the classification task layer of the SimpleView network to obtain a 40-dimensional feature vector. We have utilized the pre-trained networks based on the Github repository <sup>5</sup>.

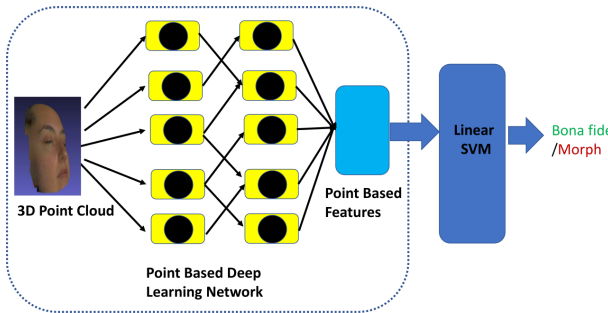


Fig. 11. Illustration of the proposed 3D face MAD

To effectively benchmark the performance of the proposed 3D MAD, we divide the newly collected dataset into two independent sets, namely training and testing. Training set consists of 3D bona fide and morphing samples from 21 unique data subjects and the testing set consists of 3D samples from 20 unique data subjects. Thus, the training set consists of 168 bona fide and 194 morphed features and the testing set consists of 160 bona fide and 151 morphed features. Table 4 shows the quantitative performance of the

5. <https://github.com/princeton-vl/SimpleView>

proposed 3D MAD techniques. Figure 12 shows the performance of individual algorithms in DET. The performance is benchmarked using ISO/IEC metrics [59] defined as Attack Presentation Classification Error Rate (APCER), which is the mis-classification rate of attack presentations and Bona fide Presentation Classification Error Rate (BPCER) is the mis-classification of bona fide presentation as attacks. In addition, we also present the results in terms of Detection Equal Error Rate (D-EER (%)). Based on the obtained results, the best performance is obtained with the SimpleView [56] network with a D-EER of 1.59%.

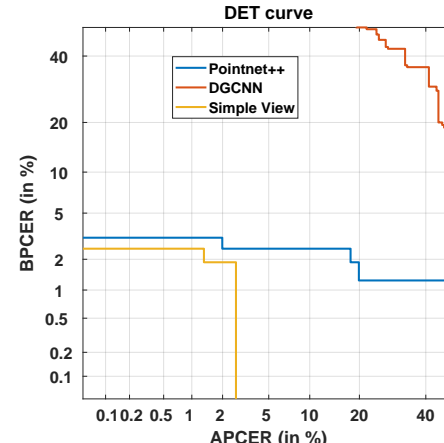


Fig. 12. DET Curve for the Proposed 3D Morphing Detection methods.

Algorithm Proposed Method	D-EER (%)	BPCER @ APCER =	
		5%	10%
Pointnet++ [47]	2.57	3.12	2.5
DGCNN [55]	37.33	81.87	68.12
SimpleView [56]	1.59	2.5	0

TABLE 4

Quantitative performance of the proposed 3D MAD techniques, performed on full dataset.

## 4 DISCUSSION

Based on the extensive experiments and obtained results made above, the research questions formulated in Section 1 are answered as below.

- **RQ#1.** Does the proposed 3D face morphing generation technique yield a high-quality 3D morphed model?

- Yes, the proposed method of generating the 3D face morphing has resulted in a high-quality morphed model almost similar to that of the original 3D bona fide. The quality analysis reported in Figure 10 and Table 3 also justifies the quality of the generated 3D morphs quantitatively as the quality values from 3D morphing show larger overlapping with the 3D bona fide. In addition, the human observer analysis reported in Section 3.2 also justifies the quality of the proposed 3D face morphing generation method as it is found reasonably difficult to detect based on the artefacts.
- **RQ#2.** Does the generated 3D face morphing model indicate the vulnerability for both automatic 3D FRS and human observers?
  - Yes, based on the analysis reported in the Section 3.3 the generated 3D face morphing model indicate a high degree of vulnerability for both automatic 3D FRS and human observers.
- **RQ#3.** Are the generated 3D face morphing models more vulnerable when compared to 2D face images for both automatic 3D FRS and human observers?
  - Equally vulnerable, the 3D face morphing models are more vulnerable than their 2D counterpart as shown in Figure 9 when using automatic FRS.
  - However, the vulnerability is almost comparable when evaluated by human observer study (see Section 3.2) where one of the main reasons could be more prevalence of 2D morphs which makes human observers sensitive about which artifacts to look for.
- **RQ#4.** Can the 3D point cloud information be used to detect the 3D face morphing attacks reliably?
  - Yes, on using the proposed 3D face morphing attack Detection approaches (see Section 3.5) the point cloud information can be used for reliable 3D morphing detection.

## 5 LIMITATIONS OF CURRENT WORK AND POTENTIAL FUTURE WORKS

Although the work presents a new dimension for face morphing attack generation and detection, especially in 3D, this work has few limitations. In the current scope of work, the 3D morph generation and detection are carried out on the high-quality 3D scans collected using the Artec Eva sensor. We have employed high-quality 3D face scans to achieve good enrolment quality scans that may reflect the real-life ID enrolment scenario. Thus, future works could investigate the proposed 3D morphing generation and detection techniques using low-quality (depth) 3D scans. Further, extending the study towards in-the-wild capture can also be considered in future work. As a second aspect, the analysis is carried out using 41 data subjects due to the present outbreak of the pandemic. However, future work can benchmark the proposed method on a large-scale dataset. As a third aspect, cleaning noise from 3D scans is tedious and sometimes requires manual intervention; thus, future work can develop a fully automated noise removal in 3D point clouds to easily the 3D morph generation.

## 6 CONCLUSION

This work presented a new dimension for face morphing attacks generation and detection, especially in 3D. We have

introduced a novel algorithm to generate high-quality 3D face morphing models using point clouds. To validate the attack potential of the newly generated 3D face morphing attacks, the vulnerability analysis is carried out using both 2D and 3D FRS. Further, the human observer analysis is also presented to investigate the usefulness of 3D information towards morph detection. Obtained results justify the high vulnerability of the proposed 3D face morphing models. We also presented an automatic quality analysis of the generated 3D morphing models that indicate a similar quality as the bona fide 3D scans. Finally, we have proposed three different 3D MAD algorithms to detect the 3D morphing attacks using pre-trained point-based CNN models. Extensive experiments indicate the efficacy of the proposed 3D MAD algorithms in detecting the 3D face morphing attacks.

## REFERENCES

- [1] F. Schroff, D. Kalenichenko, and J. Philbin, "Facenet: A unified embedding for face recognition and clustering," in *2015 IEEE Conference on Computer Vision and Pattern Recognition (CVPR)*, 2015, pp. 815–823.
- [2] J. Deng, J. Guo, N. Xue, and S. Zafeiriou, "Arcface: Additive angular margin loss for deep face recognition," in *2019 IEEE/CVF Conference on Computer Vision and Pattern Recognition (CVPR)*, 2019, pp. 4685–4694.
- [3] M. Ferrara, A. Franco, and D. Maltoni, "The magic passport," in *IEEE International Joint Conference on Biometrics*. IEEE, 2014, pp. 1–7.
- [4] R. Raghavendra, K. B. Raja, and C. Busch, "Detecting morphed face images," in *2016 IEEE 8th International Conference on Biometrics Theory, Applications and Systems (BTAS)*, 2016, pp. 1–7.
- [5] M. Ferrara, A. Franco, and D. Maltoni, "Face demorphing," *IEEE Transactions on Information Forensics and Security*, vol. 13, no. 4, pp. 1008–1017, 2017.
- [6] H. Zhang, S. Venkatesh, R. Ramachandra, K. Raja, N. Damer, and C. Busch, "Mipgan—generating strong and high quality morphing attacks using identity prior driven gan," *IEEE Transactions on Biometrics, Behavior, and Identity Science*, vol. 3, no. 3, pp. 365–383, 2021.
- [7] U. Scherhag, A. Nautsch, C. Rathgeb, M. Gomez-Barrero, R. N. Veldhuis, L. Spreeuwiers, M. Schils, D. Maltoni, P. Grother, S. Marcell *et al.*, "Biometric systems under morphing attacks: Assessment of morphing techniques and vulnerability reporting," in *2017 International Conference of the Biometrics Special Interest Group (BIOSIG)*. IEEE, 2017, pp. 1–7.
- [8] R. Raghavendra, K. Raja, S. Venkatesh, and C. Busch, "Face morphing versus face averaging: Vulnerability and detection," in *2017 IEEE International Joint Conference on Biometrics (IJCB)*. IEEE, 2017, pp. 555–563.
- [9] N. Damer, A. M. Saladié, A. Braun, and A. Kuijper, "Morgan: Recognition vulnerability and attack detectability of face morphing attacks created by generative adversarial network," in *2018 IEEE 9th International Conference on Biometrics Theory, Applications and Systems (BTAS)*. IEEE, 2018, pp. 1–10.
- [10] S. Venkatesh, H. Zhang, R. Ramachandra, K. Raja, N. Damer, and C. Busch, "Can gan generated morphs threaten face recognition systems equally as landmark based morphs?—vulnerability and detection," in *2020 8th International Workshop on Biometrics and Forensics (IWF)*. IEEE, 2020, pp. 1–6.
- [11] S. Venkatesh, R. Ramachandra, K. Raja, and C. Busch, "Face morphing attack generation & detection: A comprehensive survey," *IEEE Transactions on Technology and Society*, 2021.
- [12] M. Ngan, P. Grother, K. Hanaoka, and J. Kuo, "Part 4: Morph - performance of automated face morph detection," [https://pages.nist.gov/frvt/reports/morph/frvt\\_morph\\_report.pdf](https://pages.nist.gov/frvt/reports/morph/frvt_morph_report.pdf), 2021, [Online; accessed 16-October-2021].
- [13] A. A. Deeb, "Uae reviews features of new id card, 3d photo included," <https://www.gulftoday.ae/news/2021/08/05/uae-reviews-features-of-new-id-card-3d-photo-included>, 2020, [Online; accessed 16-October-2021].
- [14] IDEMIA, "Stereo laser image," <https://www.idemia.com/wp-content/uploads/2021/02/stereo-laser-image-idemia-brochure-202007.pdf>, 2020, [Online; accessed 18-October-2021].

[15] J. W. J. ter Hennepe, "3d photo id," [https://www.icao.int/Meetings/AMC/MRTD-SEMINAR-2010-AFRICA/Documentation/11\\_Morpho-3DPhotoID.pdf](https://www.icao.int/Meetings/AMC/MRTD-SEMINAR-2010-AFRICA/Documentation/11_Morpho-3DPhotoID.pdf), 2010, [Online; accessed 16-October-2021].

[16] D. Face Based ABC Systems, "3d face enrolment for id cards," [http://cubox.aero/cubox/php/en\\_product01-2.php?product=1/](http://cubox.aero/cubox/php/en_product01-2.php?product=1/), 2021, [Online; accessed 18-October-2021].

[17] S. Dent, "Using a 3d render as a french id card 'photo,'" <https://engt.co/3EiPnQv>, 2017, [Online; accessed 16-October-2021].

[18] ICAO, "Machine readable travel documents. part 11: Security mechanisms for mrtds. technical report doc 9303," 2021.

[19] ISO/IEC JTC1 SC37 Biometrics, "ISO/IEC 39794-5:2019 information technology — extensible biometric data interchange formats — part 5: Face image data," 2019.

[20] "Apple Face ID," [https://en.wikipedia.org/wiki/Face\\_ID](https://en.wikipedia.org/wiki/Face_ID), 2017.

[21] B. Egger, W. A. Smith, A. Tewari, S. Wuhrer, M. Zollhoefer, T. Beeler, F. Bernard, T. Bolkart, A. Kortylewski, S. Romdhani *et al.*, "3d morphable face models—past, present, and future," *ACM Transactions on Graphics (TOG)*, vol. 39, no. 5, pp. 1–38, 2020.

[22] Y. Yao, B. Deng, W. Xu, and J. Zhang, "Quasi-newton solver for robust non-rigid registration," in *Proceedings of the IEEE/CVF Conference on Computer Vision and Pattern Recognition (CVPR)*, June 2020.

[23] H. Li, R. W. Sumner, and M. Pauly, "Global Correspondence Optimization for Non-Rigid Registration of Depth Scans," *Computer Graphics Forum*, 2008.

[24] N. Gelfand, N. J. Mitra, L. J. Guibas, and H. Pottmann, "Robust global registration," in *Symposium on Geometry Processing*, 2005, pp. 197–206.

[25] B. Deng, Y. Yao, R. M. Dyke, and J. Zhang, "A survey of non-rigid 3d registration," *arXiv preprint arXiv:2203.07858*, 2022.

[26] M. Liao, Q. Zhang, H. Wang, R. Yang, and M. Gong, "Modeling deformable objects from a single depth camera," in *2009 IEEE 12th International Conference on Computer Vision*, 2009, pp. 167–174.

[27] J. Yang, D. Guo, K. Li, Z. Wu, and Y.-K. Lai, "Global 3d non-rigid registration of deformable objects using a single rgb-d camera," *IEEE Transactions on Image Processing*, vol. 28, no. 10, pp. 4746–4761, 2019.

[28] H. Li, R. W. Sumner, and M. Pauly, "Global correspondence optimization for non-rigid registration of depth scans," in *Computer graphics forum*, vol. 27, no. 5. Wiley Online Library, 2008, pp. 1421–1430.

[29] K. Zampogniannis, C. Fermüller, and Y. Aloimonos, "Topology-aware non-rigid point cloud registration," *CoRR*, vol. abs/1811.07014, 2018. [Online]. Available: <http://arxiv.org/abs/1811.07014>

[30] A. Myronenko and X. Song, "Point set registration: Coherent point drift," *IEEE transactions on pattern analysis and machine intelligence*, vol. 32, no. 12, pp. 2262–2275, 2010.

[31] G. Trappolini, L. Cosmo, L. Moschella, R. Marin, S. Melzi, and E. Rodolà, "Shape registration in the time of transformers," *Advances in Neural Information Processing Systems*, vol. 34, 2021.

[32] Y. Zeng, Y. Qian, Z. Zhu, J. Hou, H. Yuan, and Y. He, "Corrnet3d: unsupervised end-to-end learning of dense correspondence for 3d point clouds," in *Proceedings of the IEEE/CVF Conference on Computer Vision and Pattern Recognition*, 2021, pp. 6052–6061.

[33] "Artec eva sensor," <https://bit.ly/3BiGnJ1>, 2021, [Online; accessed 16-October-2021].

[34] P. Cignoni, M. Callieri, M. Corsini, M. Dellepiane, F. Ganovelli, and G. Ranzuglia, "MeshLab: an Open-Source Mesh Processing Tool," in *Eurographics Italian Chapter Conference*, V. Scarano, R. D. Chiara, and U. Erra, Eds. The Eurographics Association, 2008.

[35] B. Gärtner, "Fast and robust smallest enclosing balls," in *European symposium on algorithms*. Springer, 1999, pp. 325–338.

[36] M. Kazhdan and H. Hoppe, "Screened poisson surface reconstruction," *ACM Trans. Graph.*, vol. 32, no. 3, jul 2013. [Online]. Available: <https://doi.org/10.1145/2487228.2487237>

[37] G. Guennebaud and M. Gross, "Algebraic point set surfaces," *ACM Trans. Graph.*, vol. 26, no. 3, p. 23-es, Jul. 2007. [Online]. Available: <https://doi.org/10.1145/1276377.1276406>

[38] A. C. Oztireli, G. Guennebaud, and M. Gross, "Feature preserving point set surfaces based on non-linear kernel regression," in *Computer graphics forum*, vol. 28, no. 2. Wiley Online Library, 2009, pp. 493–501.

[39] D. E. King, "Dlib-ml: A machine learning toolkit," *Journal of Machine Learning Research*, vol. 10, pp. 1755–1758, 2009.

[40] A. Telea, "An image inpainting technique based on the fast marching method," *Journal of graphics tools*, vol. 9, no. 1, pp. 23–34, 2004.

[41] E. Rublee, V. Rabaud, K. Konolige, and G. Bradski, "Orb: An efficient alternative to sift or surf," in *2011 International Conference on Computer Vision*, 2011, pp. 2564–2571.

[42] J. D. Foley, A. Van Dam, S. K. Feiner, J. F. Hughes, and R. L. Phillips, *Introduction to computer graphics*. Addison-Wesley Reading, 1994, vol. 55.

[43] Y. Zeng, Y. Qian, Z. Zhu, J. Hou, H. Yuan, and Y. He, "Corrnet3d: Unsupervised end-to-end learning of dense correspondence for 3d point clouds," in *2021 IEEE/CVF Conference on Computer Vision and Pattern Recognition (CVPR)*, 2021, pp. 6048–6057.

[44] V. Blanz and T. Vetter, "A morphable model for the synthesis of 3d faces," in *Proceedings of the 26th annual conference on Computer graphics and interactive techniques*, 1999, pp. 187–194.

[45] T. Li, T. Bolkart, M. J. Black, H. Li, and J. Romero, "Learning a model of facial shape and expression from 4D scans," *ACM Transactions on Graphics, (Proc. SIGGRAPH Asia)*, vol. 36, no. 6, pp. 194:1–194:17, 2017. [Online]. Available: <https://doi.org/10.1145/3130800.3130813>

[46] G. Mu, D. Huang, G. Hu, J. Sun, and Y. Wang, "Led3d: A lightweight and efficient deep approach to recognizing low-quality 3d faces," in *Proceedings of the IEEE/CVF Conference on Computer Vision and Pattern Recognition (CVPR)*, June 2019.

[47] C. R. Qi, L. Yi, H. Su, and L. J. Guibas, "Pointnet++: Deep hierarchical feature learning on point sets in a metric space," *arXiv preprint arXiv:1706.02413*, 2017.

[48] P. Phillips, P. Flynn, T. Scruggs, K. Bowyer, J. Chang, K. Hoffman, J. Marques, J. Min, and W. Worek, "Overview of the face recognition grand challenge," in *2005 IEEE Computer Society Conference on Computer Vision and Pattern Recognition (CVPR'05)*, vol. 1, 2005, pp. 947–954 vol. 1.

[49] L. Yin, X. Wei, Y. Sun, J. Wang, and M. J. Rosato, "A 3d facial expression database for facial behavior research," in *7th international conference on automatic face and gesture recognition (FGR06)*. IEEE, 2006, pp. 211–216.

[50] T. Maurer, D. Guigonis, I. Maslov, B. Pesenti, A. Tsaregorodtsev, D. West, and G. Medioni, "Performance of geometrix activeid™ 3d face recognition engine on the frgc data," in *2005 IEEE Computer Society Conference on Computer Vision and Pattern Recognition (CVPR'05)-Workshops*. IEEE, 2005, pp. 154–154.

[51] U. Scherhag, A. Nautsch, C. Rathgeb, M. Gomez-Barrero, R. N. J. Veldhuis, L. Spreeuwers, M. Schils, D. Maltoni, P. Grother, S. Marcel, R. Breithaupt, R. Ramachandra, and C. Busch, "Biometric systems under morphing attacks: Assessment of morphing techniques and vulnerability reporting," in *2017 International Conference of the Biometrics Special Interest Group (BIOSIG)*, 2017, pp. 1–7.

[52] S. Venkatesh, H. Zhang, R. Ramachandra, K. Raja, N. Damer, and C. Busch, "Can gan generated morphs threaten face recognition systems equally as landmark based morphs? - vulnerability and detection," in *2020 8th International Workshop on Biometrics and Forensics (IWBF)*, 2020, pp. 1–6.

[53] FRONTEX, "Best practice technical guidelines for automated border control abc systems," 2015.

[54] Z. Zhang, "No-reference quality assessment for 3d colored point cloud and mesh models," *arXiv preprint arXiv:2107.02041*, 2021.

[55] Y. Wang, Y. Sun, Z. Liu, S. E. Sarma, M. M. Bronstein, and J. M. Solomon, "Dynamic graph CNN for learning on point clouds," *CoRR*, vol. abs/1801.07829, 2018. [Online]. Available: <http://arxiv.org/abs/1801.07829>

[56] A. Goyal, H. Law, B. Liu, A. Newell, and J. Deng, "Revisiting point cloud shape classification with a simple and effective baseline," *International Conference on Machine Learning*, 2021.

[57] Z. Wu, S. Song, A. Khosla, X. Tang, and J. Xiao, "3d shapenets for 2.5d object recognition and next-best-view prediction," *CoRR*, vol. abs/1406.5670, 2014. [Online]. Available: <http://arxiv.org/abs/1406.5670>

[58] C. R. Qi, L. Yi, H. Su, and L. J. Guibas, "Pointnet++: Deep hierarchical feature learning on point sets in a metric space," 2017. [Online]. Available: <https://arxiv.org/abs/1706.02413>

[59] ISO/IEC JTC1 SC37 Biometrics, "ISO/IEC IS 30107-3. information technology - biometric presentation attack detection - part 3: Testing and reporting," 2017.